Hindawi Publishing Corporation
Mathematical Problems in Engineering
Volume 2015, Article ID 758959, 18 pages
http://dx.doi.org/10.1155/2015/758959

Research Article

Influence of Physical and Geometrical Uncertainties in the Parametric Instability Load of an Axially Excited Cylindrical Shell

Frederico Martins Alves da Silva,[1] Augusta Finotti Brazão,[1] and Paulo Batista Gonçalves[2]

[1]*School of Civil Engineering, Federal University of Goiás, Avenida Universitária, 1488, Setor Universitário, 74605-220 Goiás, GO, Brazil*
[2]*Department of Civil Engineering, Pontifical Catholic University of Rio de Janeiro (PUC-Rio), Rua Marquês de São Vicente 225, 22451-900 Gávea, RJ, Brazil*

Correspondence should be addressed to Frederico Martins Alves da Silva; silvafma@gmail.com

Received 10 October 2014; Accepted 24 February 2015

Academic Editor: Huaguang Zhang

This work investigates the influence of Young's modulus, shells thickness, and geometrical imperfection uncertainties on the parametric instability loads of simply supported axially excited cylindrical shells. The Donnell nonlinear shallow shell theory is used for the displacement field of the cylindrical shell and the parameters under investigation are considered as uncertain parameters with a known probability density function in the equilibrium equation. The uncertainties are discretized as Hermite-Chaos polynomials together with the Galerkin stochastic procedure that discretizes the stochastic equation in a set of deterministic equations of motion. Then, a general expression for the transversal displacement is obtained by a perturbation procedure which identifies all nonlinear modes that couple with the linear modes. So, a particular solution is selected which ensures the convergence of the response up to very large deflections. Applying the standard Galerkin method, a discrete system in time domain that considers the uncertainties is obtained and solved by fourth-order Runge-Kutta method. Several numerical strategies are used to study the nonlinear behavior of the shell considering the uncertainties in the parameters. Special attention is given to the influence of the uncertainties on the parametric instability and time response, showing that the Hermite-Chaos polynomial is a good numerical tool.

1. Introduction

Theoretical and experimental results found in the literature show that cylindrical shells subjected to static loads are susceptible to buckling, and they may have a load capacity much lower than the theoretical critical load. This difference may be due to variations in physical and geometric properties [1–3], including geometric imperfections [4–6] or load noise [7, 8]. It may occur in the manufacturing process or during the service life of such structures.

The pioneering technique for quantifying the effect of randomness in problems involving structural systems was the method of Monte Carlo, which relies on repeated random sampling to obtain numerical results, that is, by running simulations many times over in order to calculate probabilities heuristically just like recording a large number of experiments [3–6, 9]. However, to access the influence of uncertainties on the nonlinear dynamics of structural systems, a large enough number of samples are necessary to obtain reliable results and, for each simulation, the equations of motion must be integrated numerically during a sufficiently long time to capture the behavior of the structure. Therefore, the Monte Carlo method requires a costly processing time. So, an alternative method not based on sampling processes is ideal for nonlinear dynamic systems.

Stochastic Galerkin method has been proposed as an alternative for solving stochastic problems. This method adapts the standard numerical methods in order to consider the uncertainties in the input parameters and to quantify their influence on the system solution. In the stochastic Galerkin method the statistical characteristics of random response, such as mean value and variance, are determined without

the need of carrying out a usually high set of samples, as shown in [10].

Recently, Sepahvand et al. [11] and Ernst et al. [12] investigated the use of polynomial chaos in various problems and studied its convergence. The method of generalized polynomial chaos with the stochastic Galerkin method has been used to analyze several stochastic problems in applied mechanics [13–18].

The nonlinear stochastic static analysis of cylindrical shells has been carried out by [19, 20] and Silva et al. [8] studied the influence of uncertainties on the nonlinear dynamic response, parametric instability boundary, bifurcation diagrams, and basins of attraction of cylindrical shells. However, none of these works uses the stochastic Galerkin method together with the expansion of the generalized polynomial chaos.

Cylindrical shells are one of the most common structural elements with applications in nearly all engineering fields. They are particularly suited to withstand axial loads and lateral pressure. Under these loading conditions thin-walled cylindrical shells usually display a complex nonlinear response due to modal coupling and interaction and high imperfection sensitivity. The study of the nonlinear vibrations of cylindrical shells goes back to the middle of the last century [21–25]. In these works either the Ritz or the standard Galerkin method is used to discretize the shell. For this, a modal expansion for the displacement field is necessary. The development of consistent modal solutions capable of describing the main modal interactions observed in cylindrical shells has received much attention in the literature. A detailed review of this subject was published by Amabili and his coauthors [26, 27].

So far, we cannot find in the literature any work that uses the stochastic Galerkin method together with the expansion of the generalized polynomial chaos to study the influence of uncertainties of physical or geometrical parameters on the nonlinear dynamics of cylindrical shells. Usually, previous works were conducted studying numerically a very large set of samples so that the results considering uncertainties in a certain parameter can be statistically reliable. But this leads to a time consuming numerical procedure [1–8]. The Galerkin method seems to be a reliable alternative, especially when only the lower bound of buckling loads is desired. Therefore, the aim of this work is to study the effects of randomness in Young's modulus, in the shells thickness, and in the amplitude of an initial geometrical imperfection on the dynamic buckling of axially excited cylindrical shell using the stochastic Galerkin method, associated with the Hermite-Chaos polynomials, and a consistent procedure to describe the nonlinear displacement field of a cylindrical shell. In this case, the proposed methodology is faster than samples' generation because the Hermite-Chaos polynomials are able to give the statistical measure without samples' generation, leading to a time efficient numerical procedure, mainly, in the study of the nonlinear dynamic response of cylindrical shells.

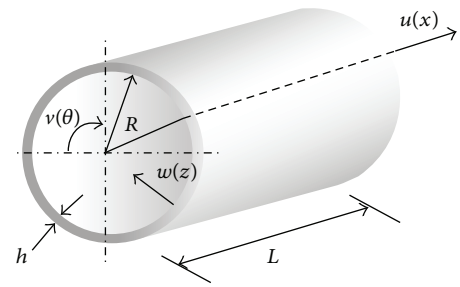

Figure 1: Geometry, coordinate system, and displacement field of the shell.

2. Problem Formulation

2.1. Deterministic Shell Equations. Consider a simply supported cylindrical shell with radius R, thickness h, and length L with an initial geometric imperfection described by a specified function w_i, made of an elastic material with Young's modulus E, Poisson coefficient υ, and density ρ. The geometry, coordinate system (x, θ, z), and displacements (u, v, w) are shown in Figure 1. The shell is subjected to an axial compressive load, $P(t)$, applied at both ends, namely, $x = 0$ and $x = L$.

Using Donnell's nonlinear shallow shell theory, the strain-displacement relations and the changes of curvature of an imperfect cylindrical shell are given by

$$\begin{aligned}
\varepsilon_x &= u_{,x} + \frac{1}{2}w_{,x}^2 + w_{,x}w_{i,x},\\
\varepsilon_\theta &= \frac{1}{R}\left(v_{,\theta} + w\right) + \frac{1}{2R^2}\left(w_{,x}^2 + w_{,\theta}w_{i,\theta}\right),\\
\gamma_{x\theta} &= v_{,x} + \frac{1}{R}\left(u_{,\theta} + w_{,x}w_{,\theta} + w_{i,x}w_{,\theta} + w_{i,\theta}w_{,x}\right),\\
k_x &= -w_{,xx},\\
k_\theta &= -\frac{1}{R^2}w_{,\theta\theta},\\
k_{x\theta} &= -\frac{1}{R}w_{,x\theta},
\end{aligned} \tag{1}$$

where ε_x, ε_θ, and $\gamma_{x\theta}$ are the midplane deformations and k_x, k_θ, and $k_{x\theta}$ are the changes of curvature of shells middle surface.

The nonlinear deterministic equations of motion based on Donnell's nonlinear shallow shell theory, in terms of a stress function f and the transversal displacement w, are given by

$$\begin{aligned}
D\nabla^4 w + 2\eta_1\rho h\omega_0\dot{w} + \eta_2 D\nabla^4\dot{w} + \rho h\ddot{w} &= \frac{1}{R}f_{,xx}\\
&+ \frac{1}{R^2}\left[f_{,xx}\left(w_{,\theta\theta} - w_{i,\theta\theta}\right) - 2f_{,x\theta}\left(w_{,x\theta} + w_{i,x\theta}\right)\right.\\
&\left.+ \left(f_{,\theta\theta} - P(t)\right)\left(w_{,xx} - w_{i,xx}\right)\right],
\end{aligned} \tag{2}$$

$$\frac{1}{Eh}\nabla^4 f = -\frac{1}{R}w_{,xx} + \frac{1}{R^2}\left[w_{,x\theta}{}^2 + 2w_{,x\theta}w_{i,x\theta} - \left(w_{,xx} + w_{i,xx}\right)w_{,\theta\theta} - w_{,xx}w_{i,\theta\theta}\right], \tag{3}$$

where η_1 and η_2 are, respectively, the linear viscous damping and the viscoelastic material damping coefficients. $D = Eh^3/12(1-\upsilon^2)$ is the flexural stiffness of the shell, ω_0 is the lowest vibration frequency, $P(t)$ is the axial load, and ∇^4 is the biharmonic operator defined as $\nabla^4 = [\partial^2/\partial x^2 + \partial^2/R^2\partial\theta^2]^2$.

The shell is subjected to a harmonic axial load, uniformly applied along the edges, of the form

$$P(t) = P_0 + P_1\cos\left(\omega_f t\right), \tag{4}$$

where P_0 is the axial static preload, P_1 is the magnitude of the axial harmonic load, ω_f is the frequency of excitation, and t is the time.

The initial geometrical imperfection is described by

$$w_i = X_{11}h\sin\left(\frac{m\pi x}{L}\right)\cos(n\theta), \tag{5}$$

where X_{11} is the amplitude of the initial geometric imperfection.

For a simply supported shell, the following boundary conditions must be satisfied in the transversal direction:

$$w(0,\theta) = w(L,\theta) = 0, \qquad M_x(0,\theta) = M_x(L,\theta) = 0. \tag{6}$$

In the foregoing, the following nondimensional parameters have been introduced:

$$W = \frac{w}{h}, \quad \tau = \omega_0 t, \quad \Omega_f = \frac{\omega_f}{\omega_0}, \quad \Gamma_0 = \frac{P_0}{P_{CR}}, \quad \Gamma_1 = \frac{P_1}{P_{CR}}, \tag{7}$$

where $P_{CR} = Eh^2/[R(3-3\upsilon^2)^{1/2}]$ is the classical axial buckling load of the shell [28, 29].

2.2. Considering Randomness at the Parameters of the Shells Equation. In this work the Young modulus (E), the shell thickness (h), and magnitude of an initial geometric imperfection (X_{11}) are considered as uncertain parameters with a known probability density function. So, these parameters introduce randomness into the nonlinear deterministic equations of motion. Considering these uncertainties, the nonlinear nondeterministic equations of motion take the form

$$\widehat{D}\nabla^4 w + 2\eta_1\rho h\omega_0\dot{w} + \eta_2 D\nabla^4\dot{w} + \rho\widehat{h}\ddot{w} = \frac{1}{R}\widehat{f}_{,xx} + \frac{1}{R^2}\left[\widehat{f}_{,xx}\left(w_{,\theta\theta} - \widehat{w}_{i,\theta\theta}\right) - 2\widehat{f}_{,x\theta}\left(w_{,x\theta} + \widehat{w}_{i,x\theta}\right) + \left(\widehat{f}_{,\theta\theta} - P(t)\right)\left(w_{,xx} - \widehat{w}_{i,xx}\right)\right], \tag{8}$$

$$\frac{1}{\widehat{E}\widehat{h}}\nabla^4\widehat{f} = -\frac{1}{R}w_{,xx} + \frac{1}{R^2}\left[w_{,x\theta}{}^2 + 2w_{,x\theta}\widehat{w}_{i,x\theta} - \left(w_{,xx} + \widehat{w}_{i,xx}\right)w_{,\theta\theta} - w_{,xx}\widehat{w}_{i,\theta\theta}\right], \tag{9}$$

where the symbol ($\widehat{\ }$) indicates that the parameter has an uncertainty with known probability density function. $\widehat{E}$ and $\widehat{h}$ are uncertainties parameters; therefore $\widehat{D} = \widehat{E}\widehat{h}^3/12(1-\upsilon^2)$ is the nondeterministic flexural stiffness and $\widehat{f}$ is the nondeterministic stress function. $\widehat{w}_i$ is the nondeterministic initial geometric imperfection because the amplitude of initial geometric imperfection (X_{11}) will be considered unknown.

2.3. General Solution of the Shell Displacement Field by a Perturbation Technique. The numerical model is developed by expanding the transversal displacement component, w, in series in the circumferential and axial variables. Previous investigations on modal solutions for the nonlinear analysis of cylindrical shells [30–34] have shown that in order to obtain a consistent modeling with a limited number of modes the chosen shape functions for the displacements must describe consistently the nonlinear displacement field of the shell and the nonlinear coupling between the modes.

By applying the perturbation procedures described in [31–34] and by considering the boundary conditions for a simply supported cylindrical shell (6) the following modal solution that accounts for the nonlinear modal coupling and the companion mode participation [26, 34] and describes consistently the vibration amplitudes up to twice the shell thickness is obtained:

$$w = \left[B_1(t)\cos(n\theta) + B_2(t)\sin(n\theta)\right]h\sin\left(\frac{m\pi x}{L}\right) + \left[B_3(t) + B_4(t)\cos(2n\theta) + B_5(t)\sin(2n\theta)\right] \cdot h\left[\frac{3}{4} - \cos\left(\frac{2m\pi x}{L}\right) + \frac{1}{4}\right] + \left[B_6(t)\cos(n\theta) + B_7(t)\sin(n\theta)\right]h \cdot \sin\left(\frac{3m\pi x}{L}\right), \tag{10}$$

where $B_i(t)$, with $i = 1, 2, \ldots, 7$, are the deterministic modal amplitude of the lateral displacement field.

The deterministic problem is solved by substituting the deterministic lateral displacement field (10), into stress function (3), and solving analytically the resulting partial differential equation. Next, substituting (10) and the obtained stress

function into the nonlinear deterministic equation of motion (2) and applying the standard Galerkin method, where the weighting functions are the trigonometric functions of (10), a set of seven nonlinear ordinary differential equations is obtained in terms of the time-dependent modal amplitudes $B_i(t)$, with $i = 1, 2, \ldots, 7$.

Now, the lateral displacements field in the nondeterministic problem defined by (8)-(9) is a random process and the time-dependent modal amplitude $B_i(t)$, with $i = 1, 2, \ldots, 7$, varies with the random parameters. So the random displacement field can be written as [10]

$$\begin{aligned} w_k^S = {} & \left[B_{1k}(t)\cos(n\theta) + B_{2k}(t)\sin(n\theta)\right] h \sin\left(\frac{m\pi x}{L}\right) \\ & + \left[B_{3k}(t) + B_{4k}(t)\cos(2n\theta) + B_{5k}(t)\sin(2n\theta)\right] \\ & \cdot h\left[\frac{3}{4} - \cos\left(\frac{2m\pi x}{L}\right) + \frac{1}{4}\right] \\ & + \left[B_{6k}(t)\cos(n\theta) + B_{7k}(t)\sin(n\theta)\right] h \\ & \cdot \sin\left(\frac{3m\pi x}{L}\right), \end{aligned} \tag{11}$$

where the amplitudes $B_{ik}(t)$, with $i = 1, 2, \ldots, 7$, are the nondeterministic modal amplitudes. The kth component in (11) is discretized using the kth Hermite-Chaos polynomial, with $k = 0, 1, \ldots, K$.

2.4. Stochastic Galerkin Method with Hermite-Chaos Polynomial. In this work the stochastic Galerkin method is applied considering an uncertainty in Young's modulus, in the shell thickness, and in the amplitude of the initial geometrical imperfection or, simultaneously, in Young's modulus and shell thickness. In the last case the random variables are considered uncorrelated. The other system parameters such as axial load, boundary conditions, and physical and geometrical properties remain constant.

The uncertainties are considered with a standard normal distribution, ϕ, given by

$$g = g_0\left(1 + \sigma_g \phi\right), \tag{12}$$

where g_0 and σ_g are, respectively, the nominal value and the variation from the nominal value of the parameter g (Young's modulus, or shell thickness, or the amplitude of the initial geometrical imperfection).

Substituting the random parameter into the nonlinear nondeterministic equation of motion, (8)-(9) become a set of stochastic partial differential equations. The stochastic Galerkin method transforms a stochastic equation into a set of deterministic differential equations where the random parameter is described by (12) and the solution is obtained by a set of Hermite-Chaos polynomials given by [10, 35]

$$w = \sum_{k=0}^{K} w_k^S \Phi_k\left(\boldsymbol{\xi}(\phi)\right), \tag{13}$$

where $\boldsymbol{\Phi}$ is the generalized polynomial chaos written in terms of the vector of N-random variables, ϕ_N. The lateral displacement field w, given by (13), is a stochastic process because the random variable introduces an uncertainty in the system.

The random variable has a normal probability density function, so the chosen orthogonal polynomials are the Hermite-Chaos polynomial [10]. The first four terms of the Hermite-Chaos polynomials, considering only one random variable, ϕ_1, are given by

$$\begin{aligned} \Phi_0 &= 1, \\ \Phi_1 &= \phi_1, \\ \Phi_2 &= \phi_1^2 - 1, \\ \Phi_3 &= \phi_1^3 - 3\phi_1, \\ \Phi_4 &= \phi_1^4 - 6\phi_1^2 + 3, \\ &\vdots \end{aligned} \tag{14}$$

The modal solution for the lateral displacement field, w given by (13), is now substituted into (9). Solving analytically the partial differential equation, a consistent solution for the stress function $\widehat{f}$ is obtained. Finally, by substituting the adopted expansion for the transversal displacement together with the obtained stress function into (8) and by applying the stochastic Galerkin method

$$\left\langle \text{Equation (8)}, \Phi_k \right\rangle = 0 \quad k = 0, \ldots, K, \tag{15}$$

a discretized deterministic system of ordinary differential equations of motion, with $(K + 1)$ equations, is derived.

The inner product between two functions given by (15) that contains only one random variable is defined as

$$\begin{aligned} & \left\langle f_1(\phi_1), f_2(\phi_1)\right\rangle \\ & \quad = \int_{-\infty}^{+\infty} \left[f_1(\phi_1) f_2(\phi_1) W(\phi_1)\right] d\phi_1, \end{aligned} \tag{16}$$

where $W(\phi_1)$ is the normal standard probability density function:

$$W(\phi_1) = \frac{1}{\sqrt{2\pi}} \exp^{-\phi_1^2/2}. \tag{17}$$

After the application of the stochastic Galerkin method given by (15), a set of deterministic equations is obtained. So, the standard Galerkin method is necessary to discretize this set of deterministic equations in the space domain, where the weighting functions are the trigonometric function of (13). Finally, a set $7 \times (K + 1)$ of nonlinear ordinary differential equations that accounts for the randomness of a given parameter is obtained in terms of the time-dependent stochastic modal amplitudes $B_{ij}(t)$, with $i = 1, 2, \ldots, 7$ and $j = 0, 1, \ldots, K$.

To consider two uncorrelated random variables simultaneously, the main changes are in the Hermite-Chaos polynomials (see [10]). The first six terms of the Hermite-Chaos

$\boldsymbol{\xi} = [\xi_0(\phi_1, \phi_2, \ldots, \phi_N), \xi_1(\phi_1, \phi_2, \ldots, \phi_N), \ldots, \xi_k(\phi_1, \phi_2, \ldots, \phi_N)]$
$\mathbf{M} = \left[\cos(n\theta)\sin\left(\frac{m\pi x}{L}\right), \sin(n\theta)\sin\left(\frac{m\pi x}{L}\right), \ldots, \sin(n\theta)\sin\left(\frac{3m\pi x}{L}\right)\right]$
to k 0, K
$\mathrm{DPDE}_k = \int_{-\infty}^{+\infty} \text{Eq. (8)}\ \xi_k(\phi_1, \phi_2, \ldots, \phi_N) W(\boldsymbol{\xi}) d\boldsymbol{\xi}$ Stochastic Galerkin method
to j 1, 7
$\mathrm{DODE}_{kj} = \int_0^L \int_0^{2\pi} \mathrm{DPDE}_k M_j R d\theta dx$ Standard Galerkin method

Pseudocode 1: Pseudocode to implement the stochastic Galerkin method associated with the standard Galerkin method.

polynomials, considering two random variables ϕ_1 and ϕ_2, are given by

$$\begin{aligned} \Phi_0 &= 1 \\ \Phi_1 &= \phi_1 \\ \Phi_2 &= \phi_2 \\ \Phi_3 &= \left(\phi_1^2 - 1\right) \\ \Phi_4 &= \phi_1\phi_2 \\ \Phi_5 &= \left(\phi_2^2 - 1\right) \\ &\vdots \end{aligned} \tag{18}$$

And the inner product for two random variables is defined as

$$\begin{aligned} &\langle f_1(\phi_1, \phi_2), f_2(\phi_1, \phi_2)\rangle \\ &= \iint_{-\infty}^{+\infty} \left[f_1(\phi_1, \phi_2) f_2(\phi_1, \phi_2) W(\phi_1, \phi_2)\right] d\phi_1 d\phi_2, \end{aligned} \tag{19}$$

where $W(\phi_1, \phi_2)$ is the normal standard probability density function for two uncorrelated random variables:

$$W(\phi_1, \phi_2) = \frac{1}{2\pi} \exp^{-((\phi_1^2/2)+(\phi_2^2/2))}. \tag{20}$$

The methodology applied in this work is presented in Pseudocode 1 where $\boldsymbol{\xi}$ is the vector that contains the kth Hermite-Chaos polynomials, as function of the N-random variable, and $\mathbf{M}$ is the vector that contains the weighting function of the standard Galerkin method. First, when the stochastic Galerkin method is applied, $(K + 1)$ deterministic partial differential equations (DPDE) are obtained. Next, for each DPDE, the standard Galerkin method is applied and $7 \times (K+1)$ deterministic ordinary differential equations (DODE) are obtained.

From the definitions about statistical moments where the first order moment is the average of random process and the second order moment is the variance of random process, it is possible to deduce the following equations [10]:

$$\begin{aligned} &E\left[\sum_{k=0}^{K} w_k^S \Phi_k(\boldsymbol{\xi}(\phi))\right] \\ &= \int \sum_{k=0}^{K} w_k^S \Phi_k(\boldsymbol{\xi}(\phi)) W(\boldsymbol{\xi}(\phi)) d\boldsymbol{\xi} \\ &= B_{i0}(t) \int \Phi_0(\boldsymbol{\xi}(\phi)) W(\boldsymbol{\xi}(\phi)) d\boldsymbol{\xi} \\ &\quad + \sum_{k=1}^{K} B_{ij}(t) \int \Phi_k(\boldsymbol{\xi}(\phi)) W(\boldsymbol{\xi}(\phi)) d\boldsymbol{\xi} \\ &= B_{i0}(t), \end{aligned} \tag{21}$$

$$\begin{aligned} &\mathrm{Var}\left[\sum_{k=0}^{K} w_k^S \Phi_k(\boldsymbol{\xi}(\phi))\right] \\ &= E\left[\sum_{k=0}^{K} w_k^S \Phi_k(\boldsymbol{\xi}(\phi))\right] \\ &\quad - \left(E\left[\sum_{k=0}^{K} w_k^S \Phi_k(\boldsymbol{\xi}(\phi))\right]\right)^2 \\ &= \sum_{k=1}^{K} {B_{ij}}^2 \int \Phi_k(\boldsymbol{\xi}(\phi)) W(\boldsymbol{\xi}(\phi)) d\boldsymbol{\xi} - {B_{i0}}^2 \\ &= \sum_{k=1}^{K} {B_{ij}}^2 \left\langle {\Phi_j}^2 \right\rangle, \end{aligned} \tag{22}$$

where (21) is the average response of each nondeterministic mode i ($i = 1, 2, \ldots, 7$) of modal solution given by (11), while the variance of each nondeterministic mode i ($i = 1, 2, \ldots, 7$) is given by (22).

3. Numerical Results

Consider a thin-walled cylindrical shell with length $L = 4$ m, radius $R = 2$ m, and nominal thickness $h_0 = 0.02$ m. The shell is made of a homogenous and isotropic material with nominal Young's modulus $E_0 = 210$ GPa, Poisson coefficient $\nu = 0.3$, and density $\rho = 7850\,\mathrm{kg/m^3}$. The linear viscous damping coefficient, η_1, is 0.001 and the viscoelastic material damping, η_2, is 0.0001. Figure 2(a) shows the variation of the vibration frequencies with the circumferential wavenumber n for selected values of the number of axial half waves m. For this geometry the lowest natural frequency occurs for vibration mode $(m, n) = (1, 5)$, identified by the symbol (●) in Figure 2(a).

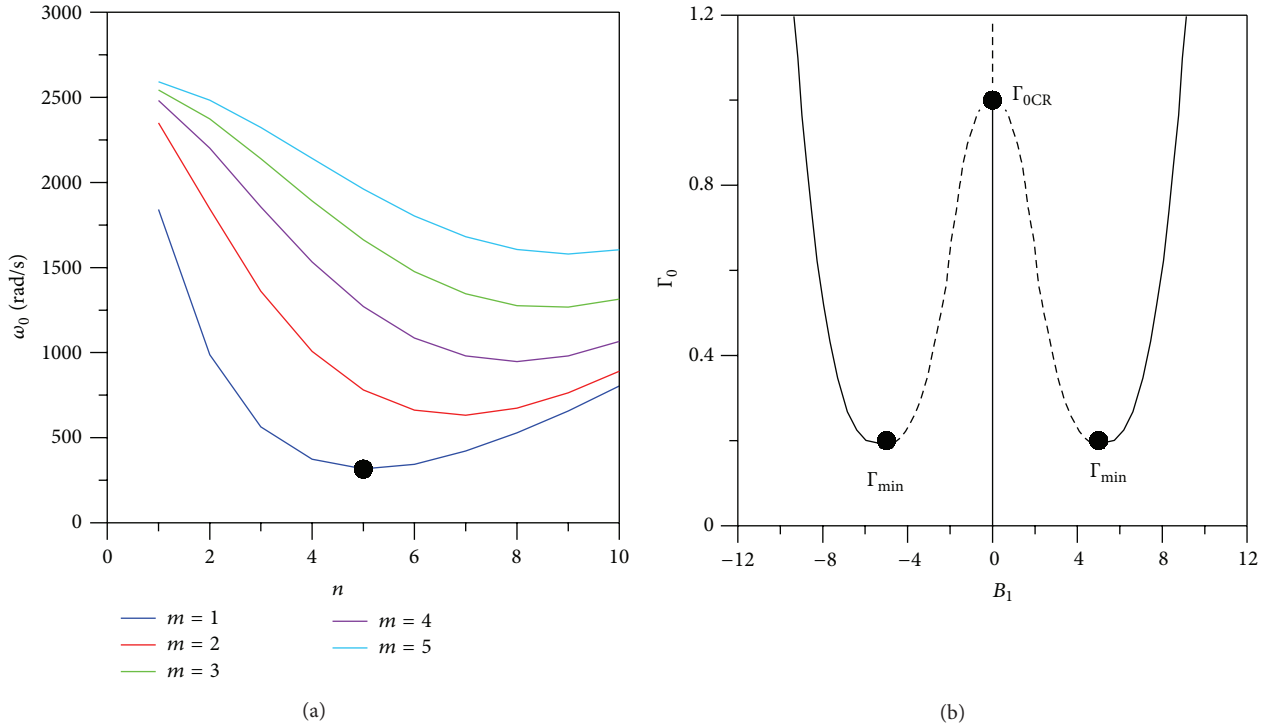

FIGURE 2: (a) Natural frequency for different vibration modes (m, n) and (b) postcritical path for the axially loaded cylindrical shell (— stable path; - - - unstable path).

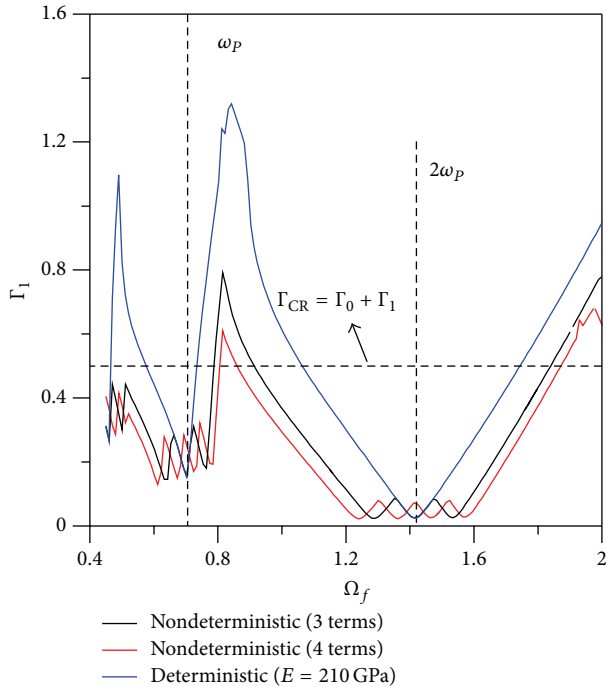

FIGURE 3: Parametric instability curves for the perfect cylindrical shell. Uncertainty in Young's modulus.

Figure 2(b) illustrates the deterministic postcritical path for the cylindrical shell under axial load with its typical initial unstable behavior until the minimum postbuckling load, Γ_{MIN}, is reached, after which the equilibrium path becomes stable. So, for any load level between the critical value, Γ_{0CR}, and Γ_{MIN} the shell has three potential wells. This figure shows the variation of the deterministic amplitude B_1 with the static preload Γ_0. For a given static preload, the cylindrical shell may

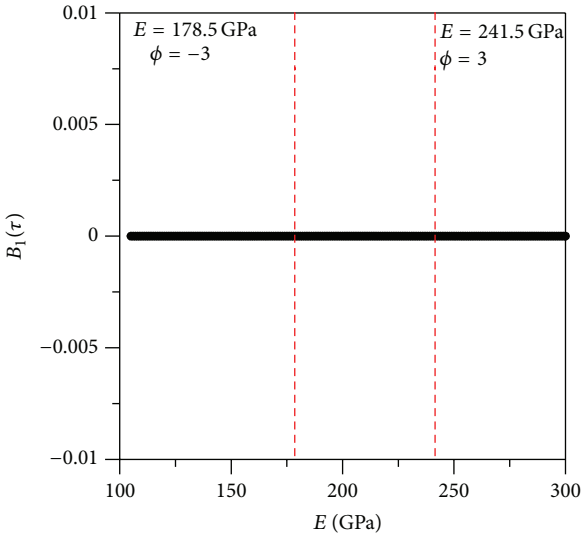

(a) $\Omega_f = 1.30$ and $\Gamma_1 = 0.01$

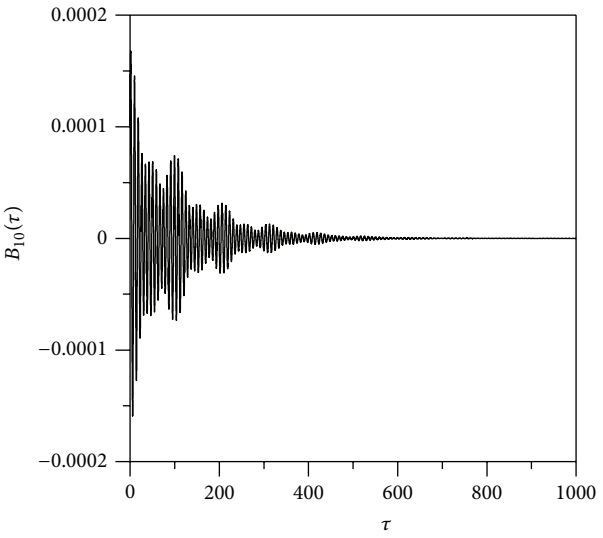

(b) $\Omega_f = 1.30$ and $\Gamma_1 = 0.01$

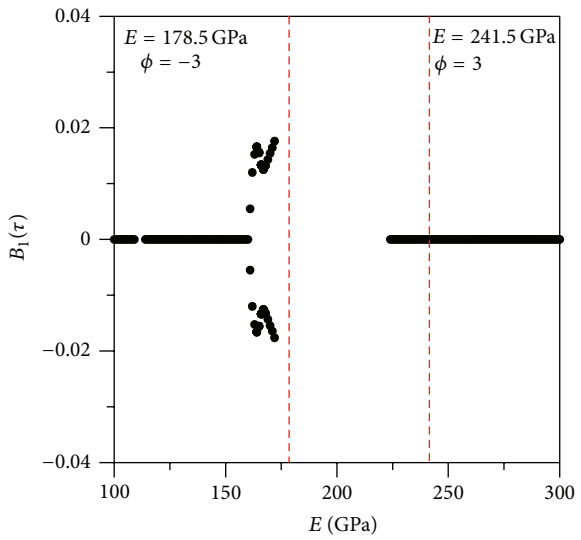

(c) $\Omega_f = 1.30$ and $\Gamma_1 = 0.30$

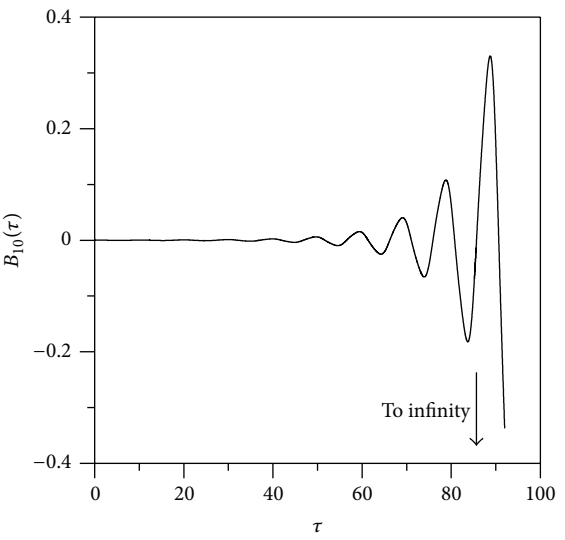

(d) $\Omega_f = 1.30$ and $\Gamma_1 = 0.30$

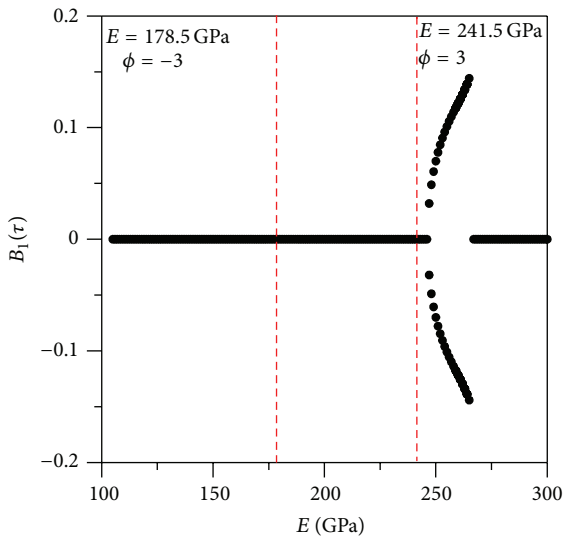

(e) $\Omega_f = 1.70$ and $\Gamma_1 = 0.10$

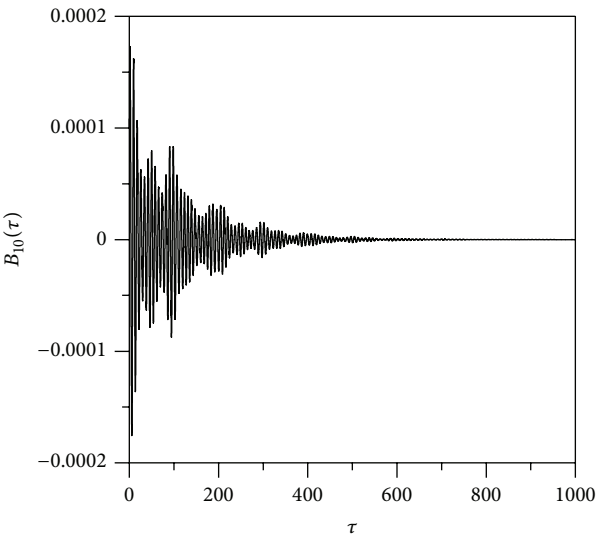

(f) $\Omega_f = 1.70$ and $\Gamma_1 = 0.10$

Figure 4: Continued.

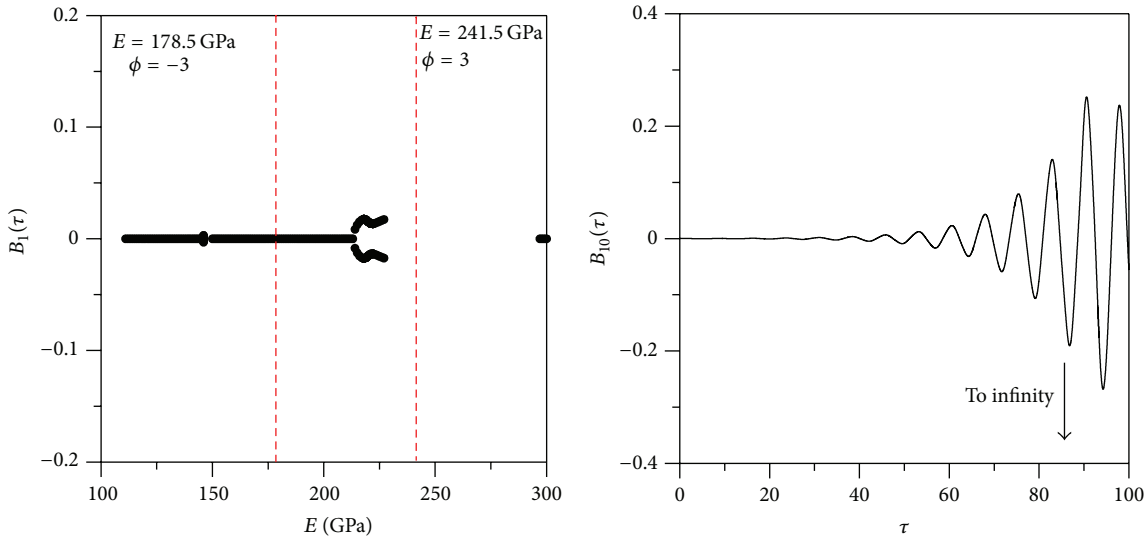

(g) $\Omega_f = 1.70$ and $\Gamma_1 = 0.40$ (h) $\Omega_f = 1.70$ and $\Gamma_1 = 0.40$

Figure 4: Deterministic bifurcation diagrams with Young's modulus as control parameter and nondeterministic time response for a perfect cylindrical shell: $\Gamma_0 = 0.50$. Four Hermite-Chaos polynomials.

escape from the prebuckling potential well (snap-through buckling). When an axial harmonic load, Γ_1, is applied a uniform forced vibration response, called breathing mode, occurs. At certain values of the axial load parameters (Γ_0, Γ_1, and Ω_f) this oscillation becomes unstable and the cylindrical shell exhibits parametric instability.

In this work, the axial preload is $\Gamma_0 = 0.50$. So, for this load, there are five static solutions: two unstable solutions and three stable solutions. The solutions within the prebuckling potential well associated with the trivial stable solution are considered the safe desired solutions.

3.1. Uncertainties in Young's Modulus. In this section a perfect cylindrical shell with random Young's modulus is considered and the other parameters remain with their design values. The uncertainty in Young's modulus is described by (12), where the nominal value, g_0 (=E_0), is 210 GPa and the adopted nominal value deviation, σ_g, is 5%. For a standard normal distribution, there are 99.6% of samples in the range $-3 < \phi < 3$. So, it is possible to assert that 99.6% of all possible samples are in the range 178.5 GPa $< g$ (=E) $<$ 241.5 GPa. Observe that this range is larger than the possible deviations expected in a standard manufacturing process.

To obtain the parametric instability boundary in the force control space (Γ_1, Ω_f), using a traditional samples' generation, for each pair (Γ_1, Ω_f), thousands of samples must be generated and its response must be obtained and next the mean value of this set of samples must be evaluated. Equation (21) guarantees the mean value directly, by the first nondeterministic modal amplitude, $B_{i0}(t)$, leading the stochastic Galerkin method to a good numerical tool that prevents the samples' generation. The numerical efficiency in comparison with samples' generation methods could be checked in works [10, 35–37].

So, the parametric instability boundary in the force control space (Γ_1, Ω_f), considering a nondeterministic problem, obtained by the stochastic Galerkin method together with the Hermite-Chaos polynomials, must be able to represent the variability of Young's modulus. The parametric instability boundaries are obtained numerically by the application of fourth order Runge-Kutta method to the discretized equations of motion. The axial harmonic excitation, Γ_1, is increased keeping constant the frequency excitation, Ω_f. When the cylindrical shell time response converges to a nontrivial steady state solution, the parametric instability load is obtained and the frequency excitation is increased.

Figure 3 shows the parametric instability boundaries for a perfect cylindrical shell considering a prestatic load $\Gamma_0 = 0.50$. The blue curve corresponds to the deterministic case while the black and red curves are obtained considering a random Young's modulus and, respectively, three and four Hermite-Chaos polynomials in (13). The horizontal dashed line indicates the cylindrical shell static critical load, while the two vertical dashed lines indicate the lowest natural frequency of the preloaded cylindrical shell considering the nominal values of Young's modulus, ω_p, and twice this value, $2\omega_p$, corresponding to secondary resonance region and main resonance region, respectively.

The region below the parametric instability boundary indicates the set of harmonic load parameters (Ω_f, Γ_1) which after a small perturbation applied to initial conditions (rest position) converges to the trivial solution. The region above the parametric instability boundaries leads to instability.

The parametric instability load of the perfect cylindrical shell with random Young's modulus, shown in Figure 3, corresponds to the highest harmonic load magnitude, Γ_1, for which the average time response remains trivial for all samples in the analyzed range; that is, there is no sample that leads to a nontrivial solution.

Figures 4(a), 4(c), 4(e), and 4(g) show for different values of Ω_f and Γ_1 the bifurcation diagrams obtained by the brute force method with Young's modulus as control parameter

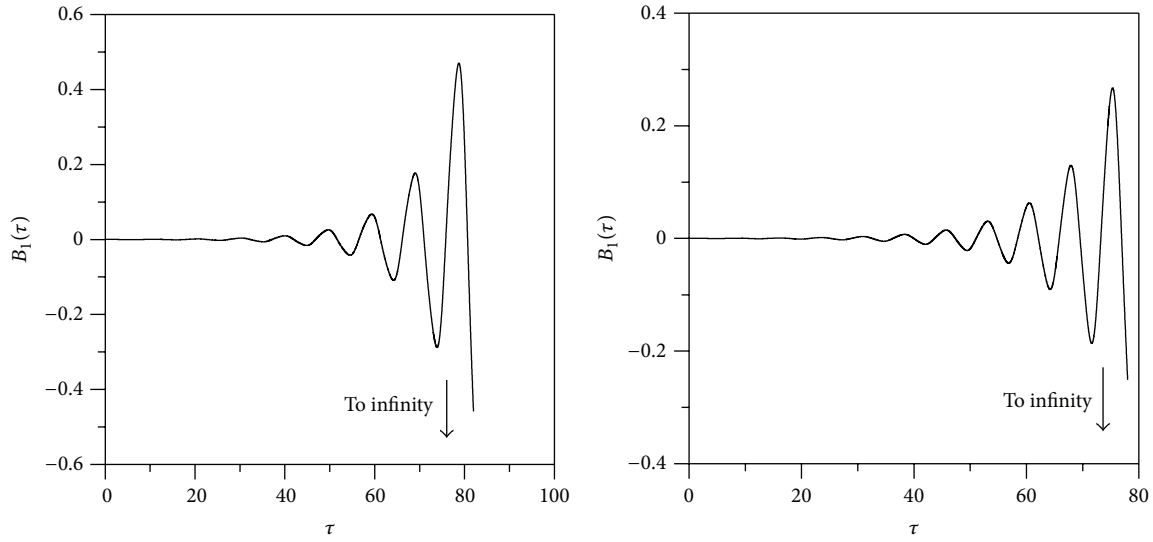

(a) $\Omega_f = 1.30$, $\Gamma_1 = 0.30$, and $E = 200$ GPa

(b) $\Omega_f = 1.70$, $\Gamma_1 = 0.40$, and $E = 235$ GPa

FIGURE 5: Deterministic time response illustrating the influence of the uncertainties in Young's modulus: $\Gamma_0 = 0.50$.

(100 GPa $< E <$ 300 GPa). The range $-3 < \phi < 3$ (178.5 GPa $< E <$ 241.5 GPa) is indicated in these figures by the two vertical dashed red lines which contains 99.6% of all possible samples. Figures 4(b), 4(d), 4(f), and 4(h) show the average nondeterministic time response of the fundamental vibration mode, $B_{10}(\tau)$, for the same values of Ω_f and Γ_1 indicated in the deterministic bifurcation diagrams of Figures 4(a), 4(c), 4(e), and 4(g). As observed in Figures 4(c) and 4(g), there is a region between the vertical red lines where there is no stable solution because the time response for at least a sample in this region goes to infinity, as illustrated in Figure 5. So, the average of the time response goes to infinity too. Now, in Figures 4(a) and 4(e) the deterministic bifurcation diagram is stable within the analyzed range. In these cases, the average of the time response is zero, as shown in Figures 4(b) and 4(f).

The nondeterministic time responses in Figure 4 agree with the nondeterministic parametric instability boundary of Figure 3. Due to Young's modulus uncertainty, there is a noticeable decrease in the parametric instability boundary. Increasing the number of Hermite-Chaos polynomials, the discretization of the probability density function becomes more accurate, since more samples are included in the analysis, leading to a further (small) decrease in the load capacity of the shell. The selection of the order of polynomial chaos expansion was conducted through a convergence analysis by observing the numerical difference between the values of the parametric instability load of the current order with the previous one. The current order was assumed to be good enough when this difference was less than 5%.

3.2. Uncertainties in the Shells Thickness. Now, in this section the uncertainties in the shell thickness are considered and the other parameters are assumed with their design values. The uncertainties in the shell thickness are described in (12), where the nominal value, g_0 (=h_0), is 0.02 m and the adopted nominal value deviation, σ_g, is 2.5% (small variation in the shell thickness). Figure 6 shows the parametric instability boundaries for the deterministic case and the nondeterministic case considering three and four Hermite-Chaos polynomials in (13). The parametric instability load decreases due to the variation of the shell thickness. Among the shell geometrical parameters (L, R, and h), the thickness is the most critical, since small variations in the shell thickness may cause a significant decrease in the stability boundary and the maximum variation must thus be prescribed in design. Also,

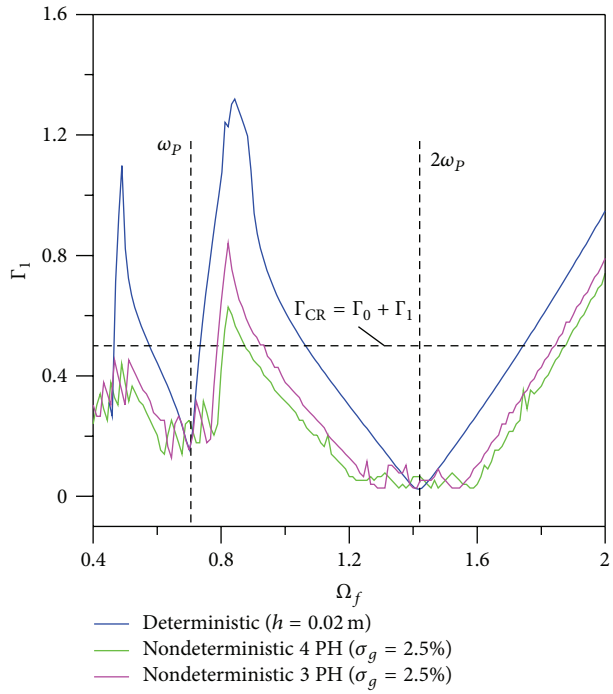

FIGURE 6: Parametric instability boundaries considering uncertainty in the shell thickness.

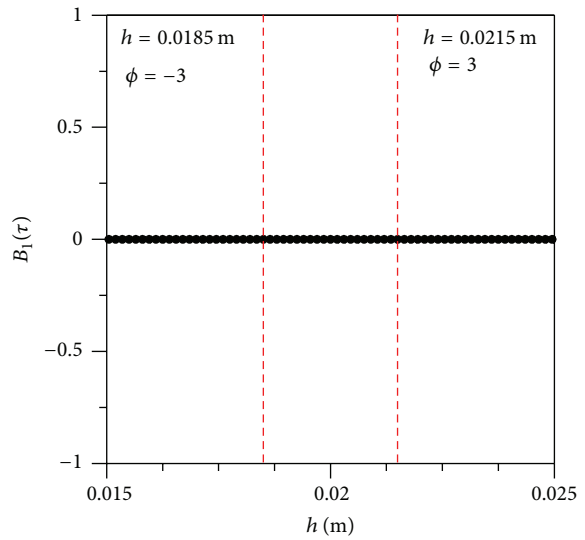

(a) $\Omega_f = 1.30$ and $\Gamma_1 = 0.01$

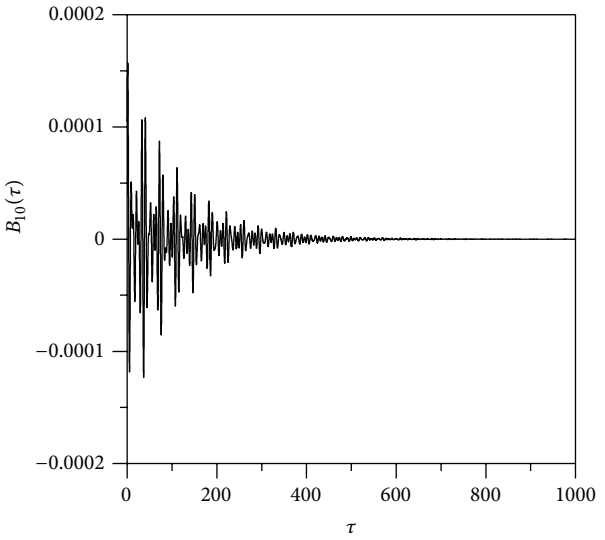

(b) $\Omega_f = 1.30$ and $\Gamma_1 = 0.01$

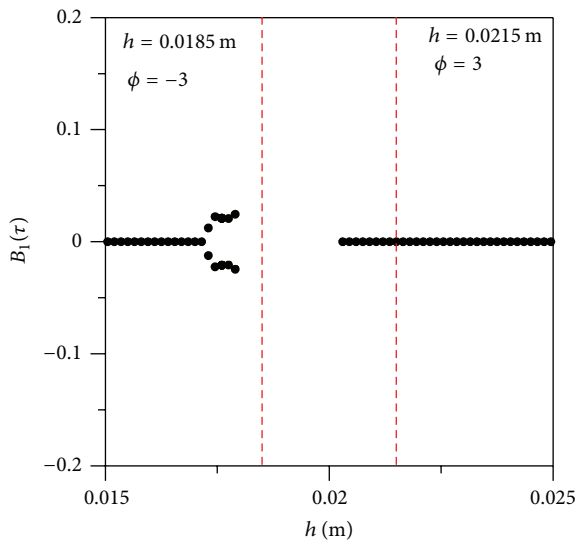

(c) $\Omega_f = 1.30$ and $\Gamma_1 = 0.20$

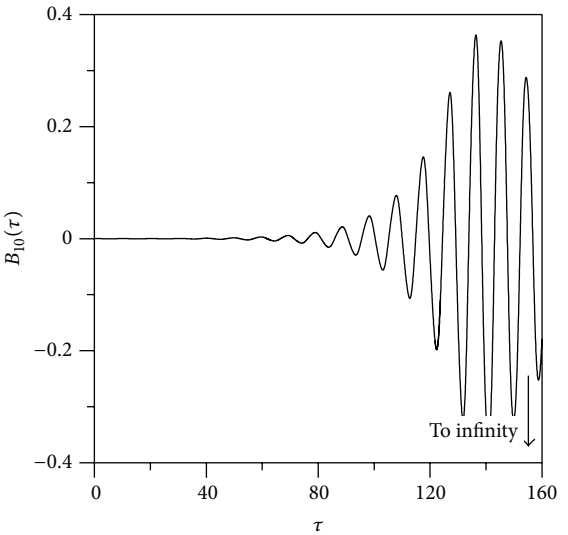

(d) $\Omega_f = 1.30$ and $\Gamma_1 = 0.20$

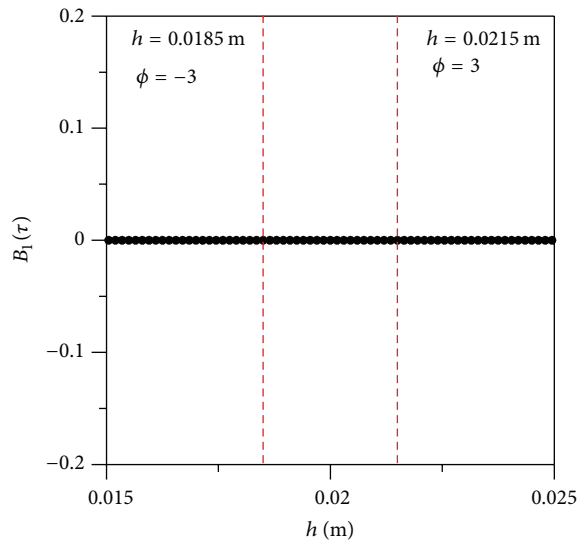

(e) $\Omega_f = 1.70$ and $\Gamma_1 = 0.01$

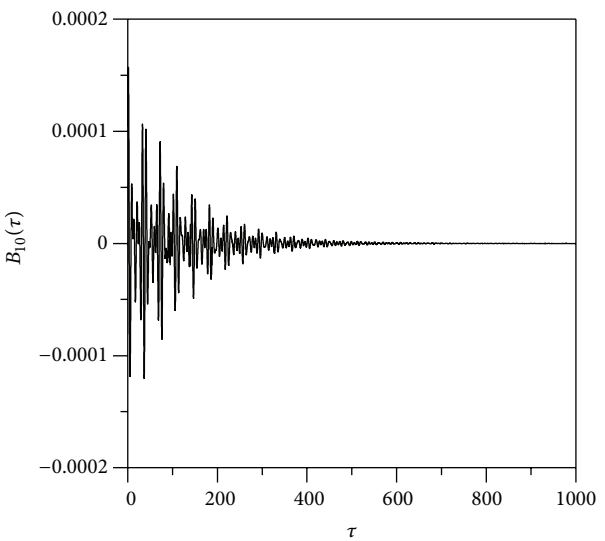

(f) $\Omega_f = 1.70$ and $\Gamma_1 = 0.01$

Figure 7: Continued.

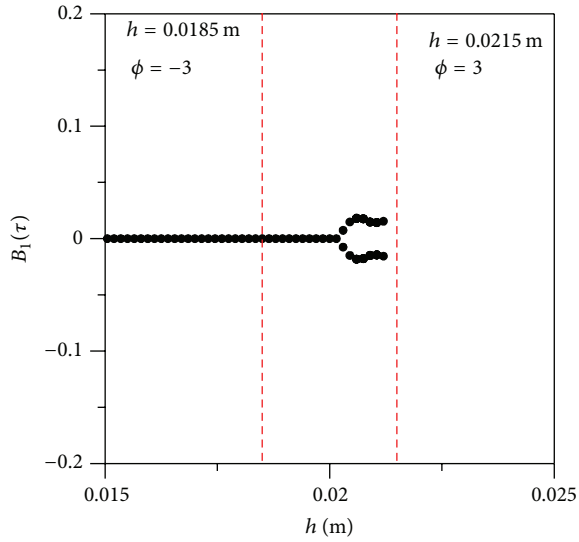

(g) $\Omega_f = 1.70$ and $\Gamma_1 = 0.40$

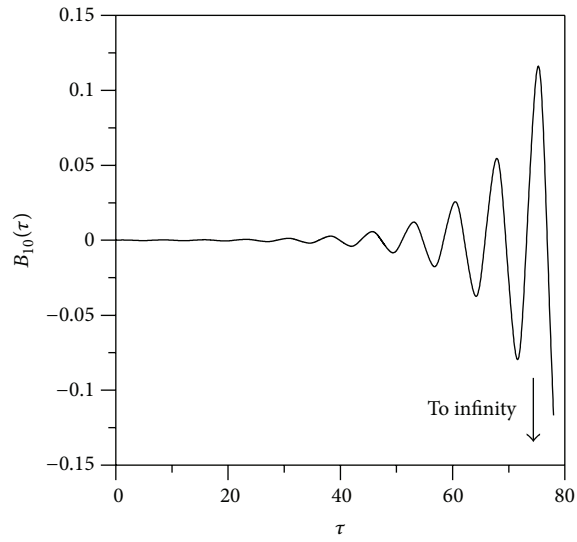

(h) $\Omega_f = 1.70$ and $\Gamma_1 = 0.40$

FIGURE 7: Bifurcation diagrams having as control parameter the shell thickness and average time responses for select load parameter values: $\Gamma_0 = 0.50$ and $\sigma_g = 8.33\%$. Four Hermite-Chaos polynomials.

as in the case of Young's modulus (Figure 3), a lower bound around $2\omega_P$, nearly equal to the minimum critical load of the perfect system, is observed. This can be prescribed as a conservative lower bound in the resonance regions.

Figures 7(a), 7(c), 7(e), and 7(g) present, for selected values of the load excitation, the bifurcation diagrams having as a control parameter the shells thickness. The dashed red lines indicate the considered range of variation of the shells thickness, $0.0185\,\text{m} < h < 0.0215\,\text{m}$, which contains 99.6% of all samples considering a standard normal distribution with nominal value deviation, σ_g, equal to 2.5%. It should be pointed out that similar instability boundaries are obtained using different distributions. However, for each distribution, a different family of chaos polynomials must be selected [10, 35].

Figures 7(b), 7(d), 7(f), and 7(h) illustrate, respectively, the average of the time response of each bifurcation diagram given by Figures 7(a), 7(c), 7(e), and 7(g). As observed in the analysis of the cylindrical shell with uncertainties in Young's modulus, if the bifurcation diagram has a region with only stable solution in the analyzed range (between the red dashed vertical lines), the average of the time response goes to a trivial solution, as given by Figures 7(b) and 7(f). Now, if the bifurcation diagram has a region with unstable solution in the analyzed range, the average of the time response goes to infinity, as shown by Figures 7(d) and 7(h).

As also observed in the analyses with uncertainties in Young's modulus (Figure 3), increasing the number of Hermite-Chaos polynomials, the discretization of the probability density function of the uncertainty becomes more accurate, since a larger number of samples are included in the analysis.

3.3. Uncertainties in the Magnitude of the Initial Geometric Imperfection. Initial imperfections are a key issue in the stability analysis of cylindrical shells. Now the influence of an uncertainty in the magnitude of the initial geometric imperfection, X_{11}, is investigated. For this, X_{11} is assumed as the random variable with a normal standard probability density function given by (12) and the nominal values for other geometrical and physical parameters. The initial geometric imperfection is considered to vary in the range $-0.75 < X_{11} < 0.75$ ($-3 < \phi < 3$), which is within the range

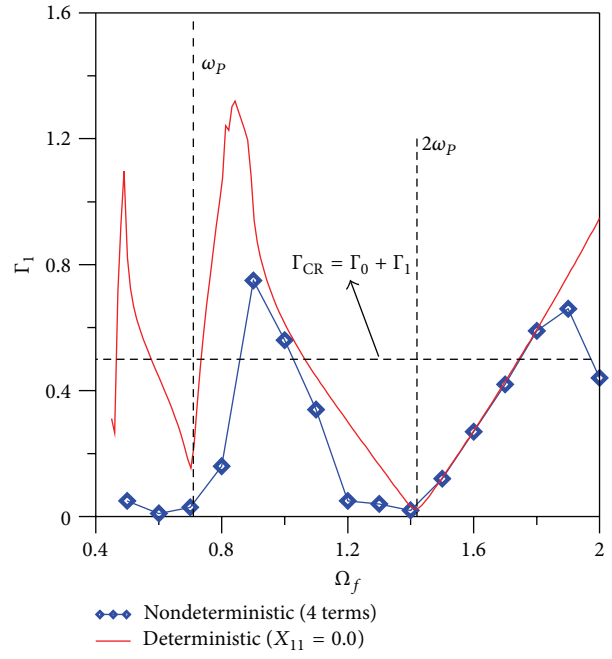

FIGURE 8: Parametric instability boundaries for the cylindrical shell. Uncertainty in the magnitude of initial geometric imperfection: $\Gamma_0 = 0.50$.

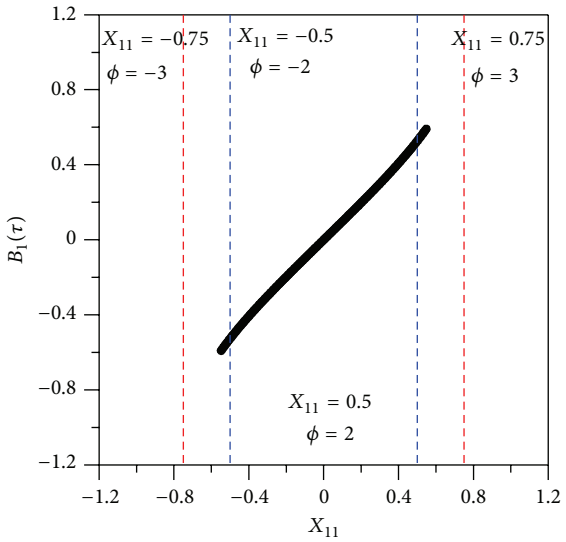

(a) $\Omega_f = 1.30$ and $\Gamma_1 = 0.01$

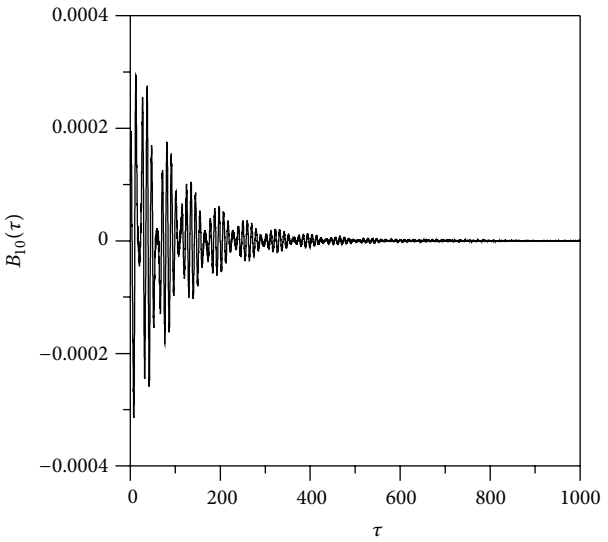

(b) $\Omega_f = 1{,}30$ and $\Gamma_1 = 0.01$

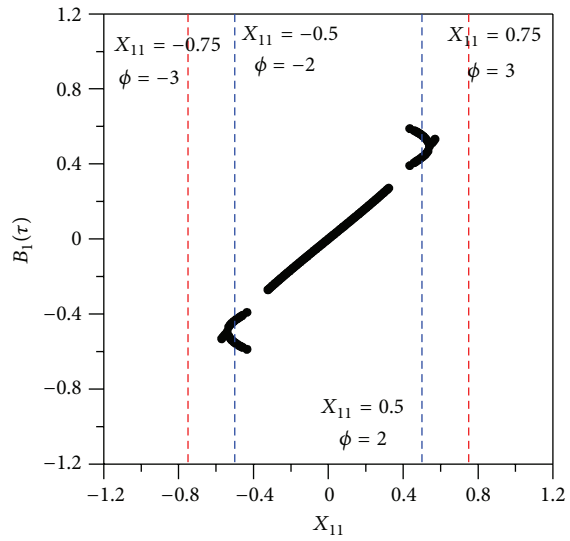

(c) $\Omega_f = 1.30$ and $\Gamma_1 = 0.20$

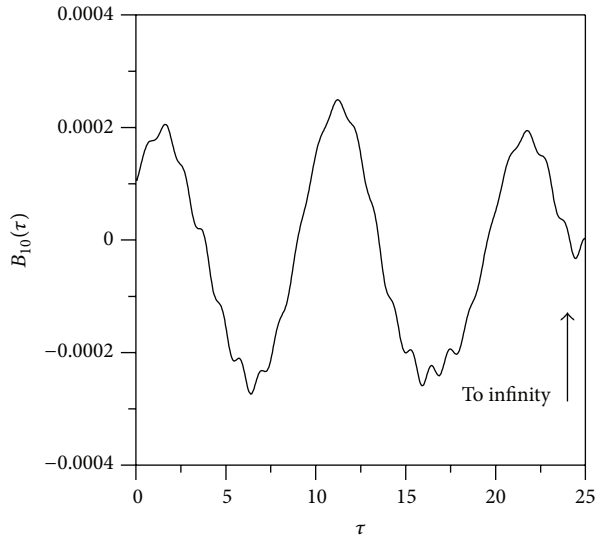

(d) $\Omega_f = 1.30$ and $\Gamma_1 = 0.20$

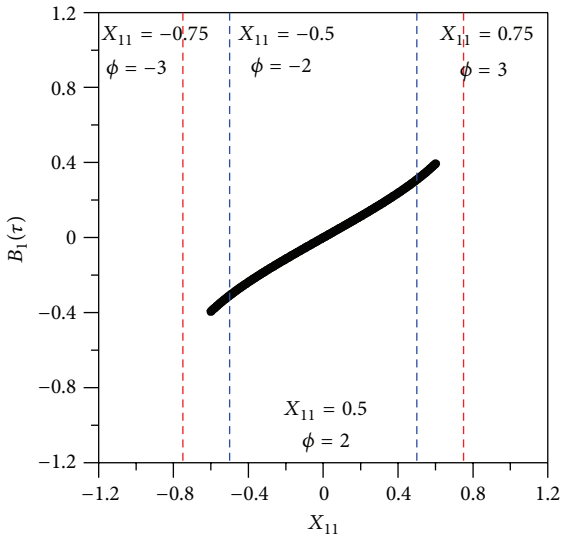

(e) $\Omega_f = 1.70$ and $\Gamma_1 = 0.40$

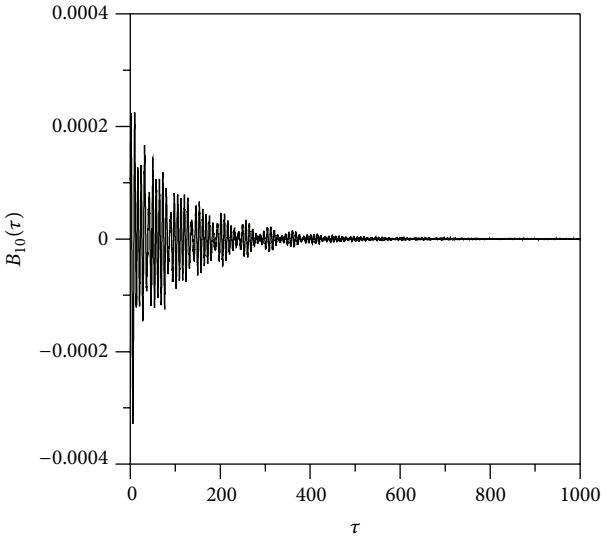

(f) $\Omega_f = 1.70$ and $\Gamma_1 = 0.40$

Figure 9: Continued.

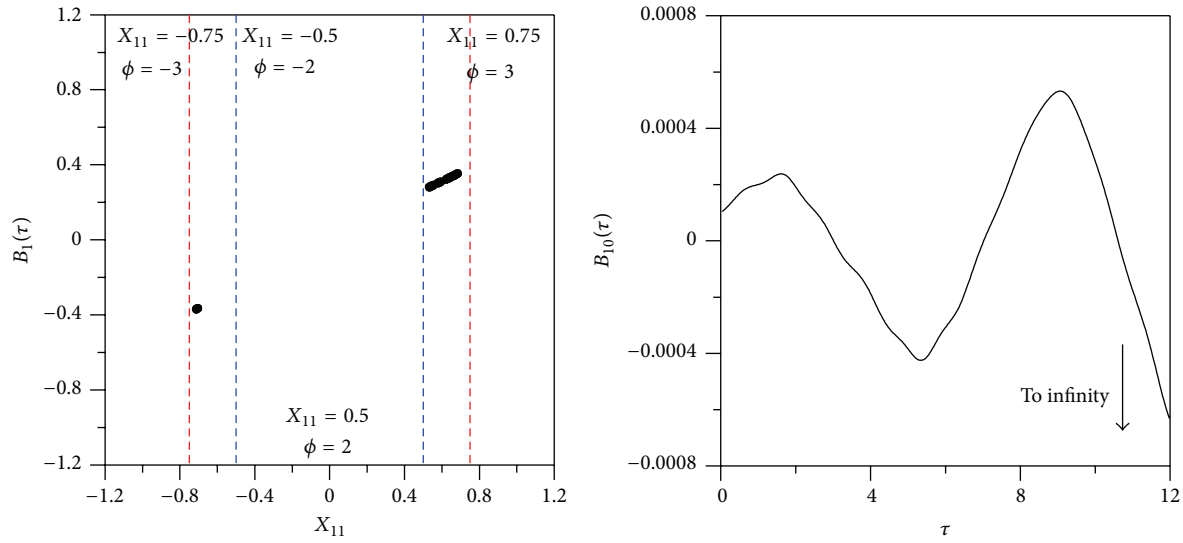

(g) $\Omega_f = 1.70$ and $\Gamma_1 = 0.60$ (h) $\Omega_f = 1.70$ and $\Gamma_1 = 0.60$

FIGURE 9: Bifurcation diagrams with amplitude of initial geometric imperfection as control parameter and time responses: $\Gamma_0 = 0.50$.

prescribed by most design codes, considering a nominal value for the initial geometric imperfection, g_0 in (12), equal to zero (perfect shell) and $\sigma_g = 0.25$. This range encompasses 99.6% of all samples. Initially, Figure 8 compares the parametric instability boundary for a perfect cylindrical shell under axial excitation and the parametric instability boundary for an imperfect cylindrical shell, considering a normal probability density function. The lower bound of critical loads for the imperfect shell is in agreement with the imperfection sensitivity analysis presented in [32, 38].

Figures 9(a), 9(c), 9(e), and 9(g) display the bifurcation diagrams having as control parameters the magnitude of the imperfection, while Figures 9(b), 9(d), 9(f), and 9(h) show the time response for selected values of Ω_f and Γ_1. It can be observed that, in the interval where no stable solution occurs (see Figures 9(c) and 9(g)), the mean time response goes to infinity (Figures 9(d) and 9(h)) because there is at least one value of imperfection whose time response is unstable (escape from the prebuckling well).

It is possible to notice in Figures 9(a) and 9(e) that there are unstable solutions in the range $-3 < \phi < 3$ and their respective mean time response should go to infinity but they go to a trivial solution. In Figures 9(a) and 9(e) in the interval $-2 < \phi < 2$ all solutions are stable. Figures 9(b) and 9(f) show a good prediction of nondeterministic time response for the range $-2 < \phi < 2$ that encompasses 95.4% of all samples. In this range there are only stable solutions and the average response converges to the trivial solution. However, in the ranges $-3 < \phi < -2$ and $2 < \phi < 3$ instabilities are observed. In these cases, the respective nondeterministic time responses, as in Figures 9(b) and 9(f), should go to infinity, but they converge to the trivial response. This is due to the number of Hermite-Chaos polynomials used in the analysis.

To obtain a correct time response of Figures 9(b) and 9(f), the first five Hermite-Chaos polynomials (13) are used and the correct nondeterministic time response for the range $-3 < \phi < 3$ can be obtained, as in Figure 10. So, to detect the instability in the analyzed range a larger number of Hermite polynomials are required.

3.4. Uncorrelated Uncertainties in Young's Modulus and Shell Thickness. In this section the effect of a simultaneous and uncorrelated uncertainty in Young's modulus and in shells thickness is analyzed. For this, the random transversal field displacement given by (13) is discretized with the Hermite-Chaos polynomials shown in (18) that contain two random variables, ϕ_1 and ϕ_2, and six polynomials' functions. The uncertainty in Young's modulus is described as in (12), where the nominal value, g_0 $(=E_0)$, is 210 GPa and the adopted nominal value deviation, σ_g, is 5%. The uncertainties in the shell thickness are described in (12), where the nominal value, g_0 $(=h_0)$, is 0.02 m and the adopted nominal value deviation, σ_g, is 2.5%.

Figure 11 shows the parametric instability boundaries for a perfect cylindrical shell under a prestatic load $\Gamma_0 = 0.50$. The blue parametric instability boundary is obtained considering a deterministic problem (nominal values) while the black parametric instability boundary is obtained considering a simultaneous and uncorrelated uncertainty in Young's modulus and in shells thickness. To identify the main changes caused by the simultaneous uncertainties, the parametric instability boundaries considering only Young's modulus randomness (green boundary) or the shells thickness uncertainties (red boundary) are also shown in Figure 11.

To analyze the simultaneous influence of the uncorrelated uncertainty in Young's modulus and shell thickness on the parametric instability boundary, the deterministic time response for each pair of deterministic parameters in the normalized plane E/E_0 versus h/h_0 is investigated, as shown in Figures 12(a), 12(c), 12(e), and 12(g), where E_0 and h_0 are the reference values. The red straight continuous lines indicate the chosen range for both parameters that contain

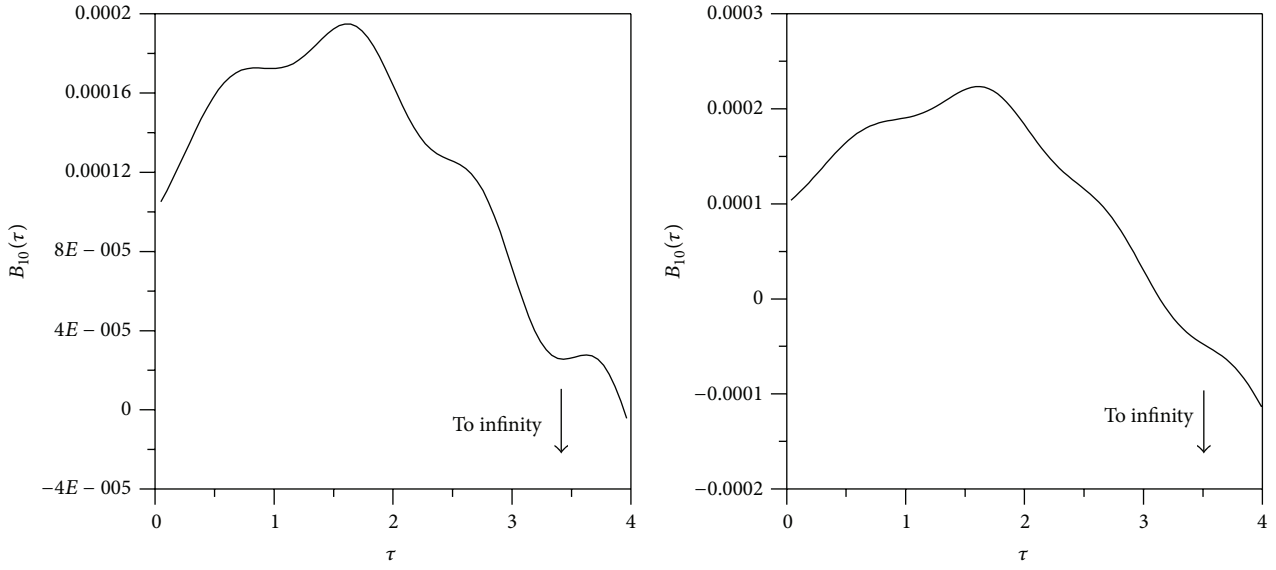

(a) $\Omega_f = 1.30$ and $\Gamma_1 = 0.01$ (b) $\Omega_f = 1.70$ and $\Gamma_1 = 0.40$

FIGURE 10: Nondeterministic time response considering the first five Hermite-Chaos polynomials for an imperfect cylindrical shell: $\Gamma_0 = 0.50$.

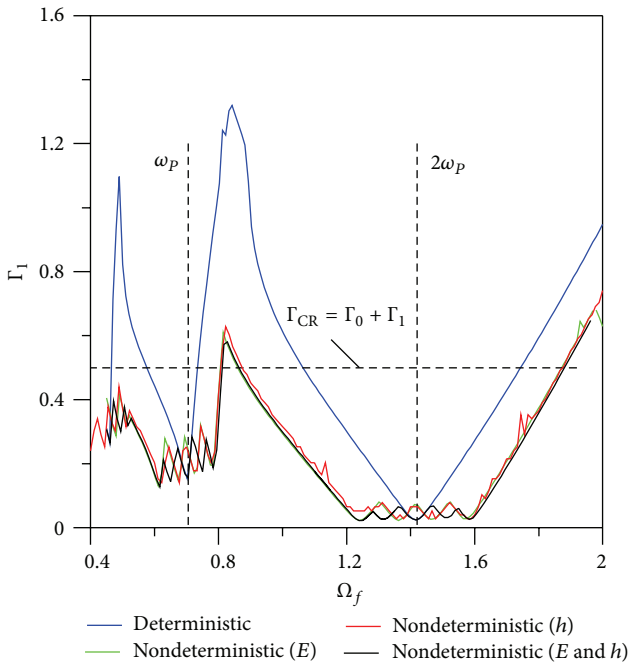

FIGURE 11: Parametric instability boundaries considering uncertainty in Young's modulus and shell thickness: $\Gamma_0 = 0.50$.

99.6% of all possible samples. The aim of these mappings is to determine which combinations of Young's modulus and shells thickness, for a certain harmonic load, are stable and which combinations are unstable solutions. For every stable solution, in those figures, the pairs $(E/E_0, h/h_0)$ are plotted in black, while the unstable solutions are plotted in white. Figure 13(a) illustrates a pair $(E/E_0, h/h_0)$ (yellow point in Figure 12(a)) that leads to a stable trivial solution, while Figure 13(b) illustrates a pair $(E/E_0, h/h_0)$ (green point in Figure 12(a)) for which the response is unstable.

Figures 12(b), 12(d), 12(f), and 12(h) represent the time responses corresponding, respectively, to Figures 12(a), 12(c), 12(e), and 12(g). From Figures 12(a) and 12(e) one can conclude that in the chosen range (region inside the red continuous lines) only stable solutions exist and the nondeterministic time response must be stable, as illustrated in Figures 12(b) and 12(f). In Figures 12(c) and 12(g) there are regions with unstable solutions (white region) inside the chosen range and the time responses are unstable, as shown in Figures 12(d) and 12(h). So, the present methodology has been shown to be a good numerical tool to evaluate the parametric instability boundaries for problems with one or more random variables.

4. Conclusions

In this work the influence of uncertainties in Young's modulus of the shell material, shell thickness, and magnitude of initial geometric imperfection or the parametric instability boundaries of an axially excited cylindrical shell is analyzed. The Donnell nonlinear shallow shell theory is used to study the nonlinear vibrations of the shell. To solve the stochastic differential equation, the uncertainties are discretized using Hermite-Chaos polynomials and the stochastic Galerkin method is applied to obtain a set of deterministic partial differential equations of motion, which are solved by the Runge-Kutta method. A modal expansion for the transverse displacement field is obtained using perturbation techniques. This expansion includes all nonlinear modes which couple with the linear modes through quadratic and cubic nonlinearities in the nonlinear equations of motion. A particular solution of this expansion, satisfying all boundary conditions, is selected in such a way as to guarantee the convergence

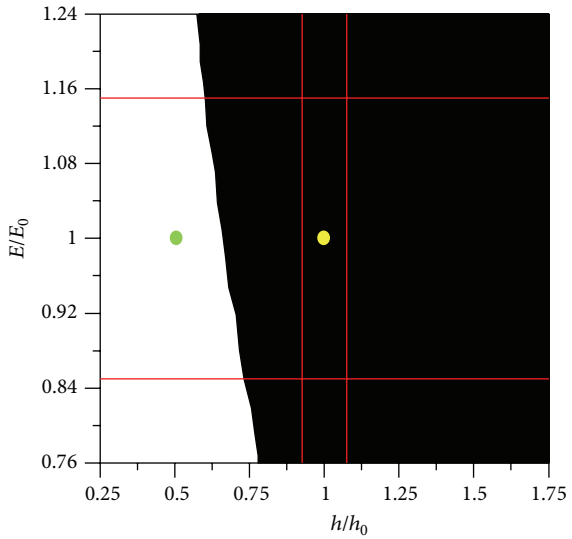

(a) $\Omega_f = 1.30$ and $\Gamma_1 = 0.01$

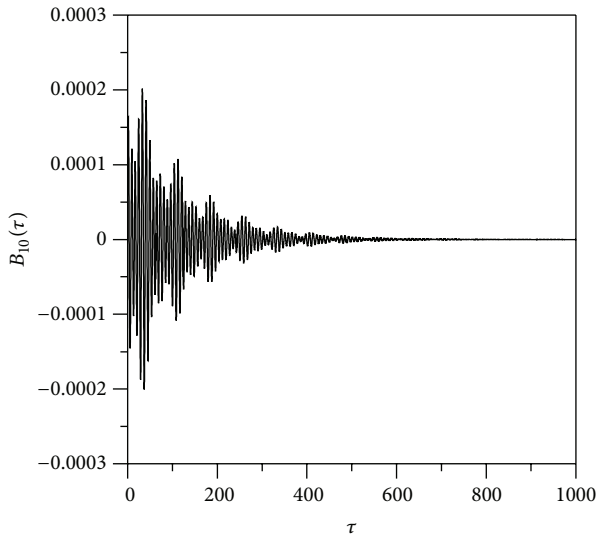

(b) $\Omega_f = 1.30$ and $\Gamma_1 = 0.01$

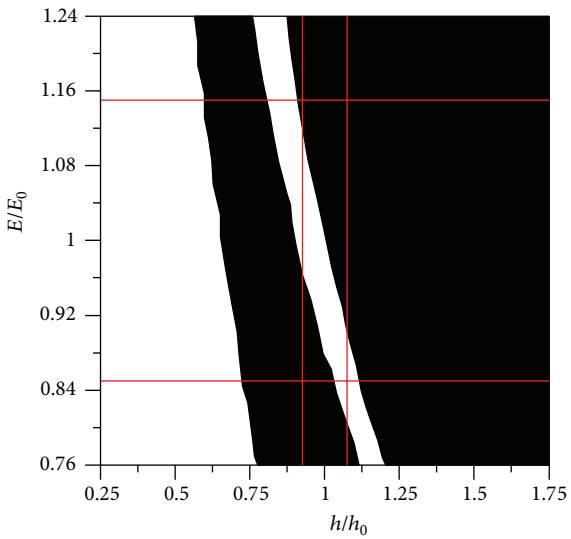

(c) $\Omega_f = 1.30$ and $\Gamma_1 = 0.20$

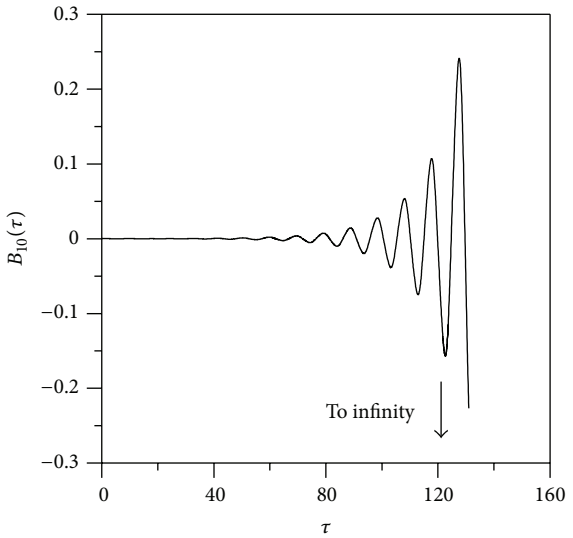

(d) $\Omega_f = 1.30$ and $\Gamma_1 = 0.20$

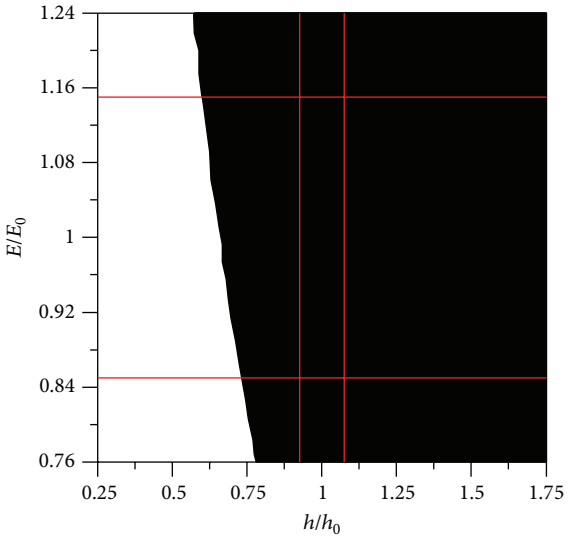

(e) $\Omega_f = 1.70$ and $\Gamma_1 = 0.01$

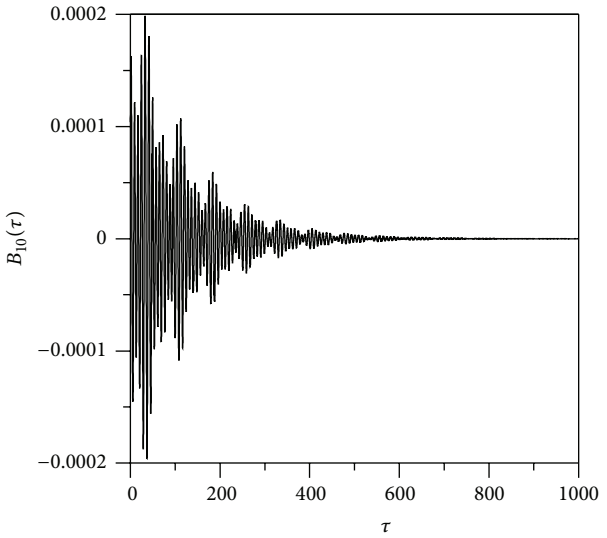

(f) $\Omega_f = 1.70$ and $\Gamma_1 = 0,01$

Figure 12: Continued.

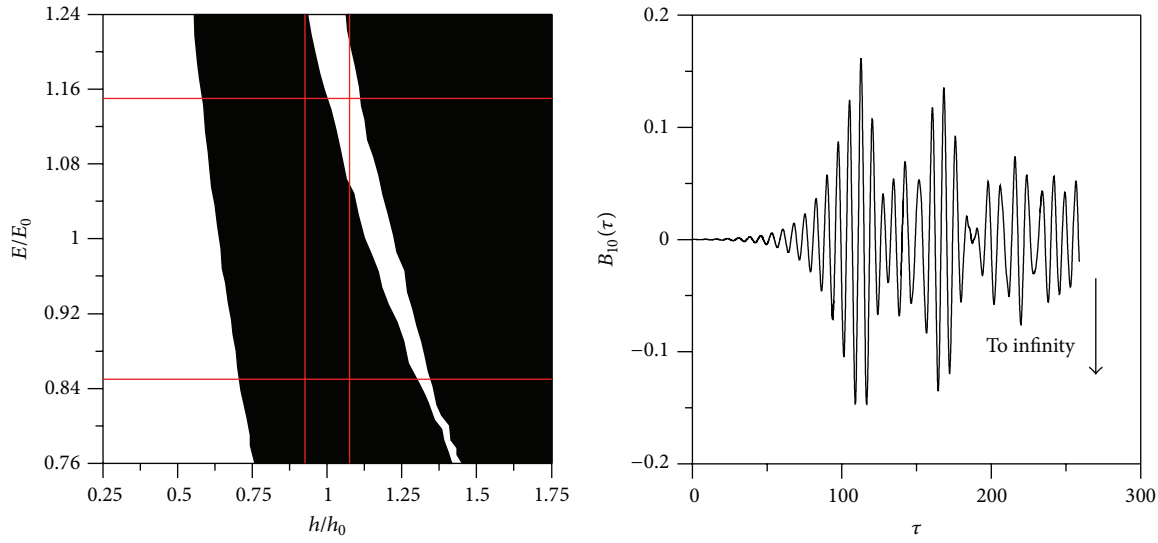

(g) $\Omega_f = 1.70$ and $\Gamma_1 = 0.30$ (h) $\Omega_f = 1.70$ and $\Gamma_1 = 0.30$

FIGURE 12: Mapping the stable solution and the nondeterministic time response with simultaneous and uncorrelated uncertainties in Young's modulus and shells thickness: $\Gamma_0 = 0.50$.

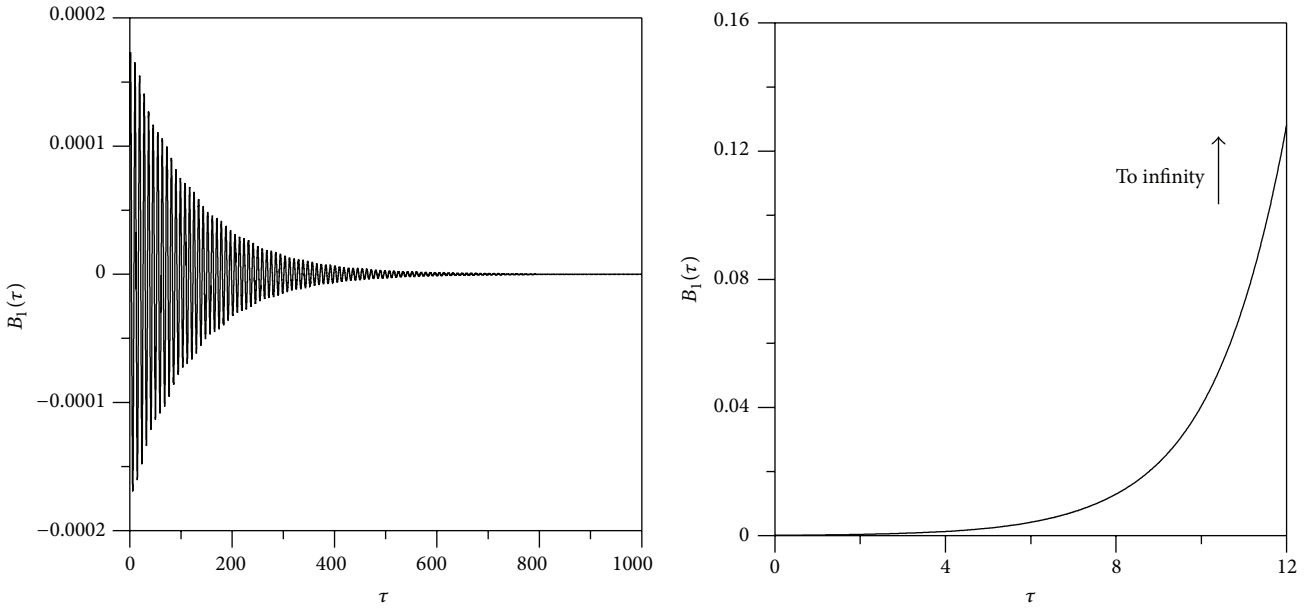

(a) $E = 210$ GPa and $h = 0.02$ m (b) $E = 210$ GPa and $h = 0.01$ m

FIGURE 13: Deterministic time response for different values of Young's modulus and shells thickness: $\Gamma_0 = 0.50$, $\Omega_f = 1.30$, and $\Gamma_1 = 0.01$.

of the response even to large vibration amplitudes. The results show that this procedure is able to quantify the influence of the uncertainties on the instability boundaries of the axially loaded cylindrical shell. The present results show that the parametric instability boundaries of non-deterministic systems are the lower bound of the results considering uncertainties in a given parameter. This indicates that the Hermite-Chaos polynomials are a good alternative to describe the randomness of a partial differential equation in stochastic nonlinear dynamics when the random variable is described by a standard normal distribution. Additional studies on the use of polynomial chaos in nonlinear dynamics field, mainly other random distribution and the possibility of application of the generalized polynomials chaos, are indicated, for example, to study which is the influence of uncertainties on bifurcations and erosion of the basins of attraction of a nonlinear dynamical system.

Conflict of Interests

The authors declare that there is no conflict of interests regarding the publication of this paper.

Acknowledgments

This work was made possible by the support of the Brazilian Ministry of Education CAPES, CNPq, FAPERJ-CNE, and FAPEG.

References

[1] D. Yadav and N. Verma, "Buckling of composite circular cylindrical shells with random material properties," *Composite Structures*, vol. 37, no. 3-4, pp. 385–391, 1997.

[2] B. N. Singh, D. Yadav, and N. G. R. Iyengar, "Initial buckling of composite cylidrical panels with random material properties," *Composite Structures*, vol. 53, no. 1, pp. 55–64, 2001.

[3] V. Papadopoulos, G. Stefanou, and M. Papadrakakis, "Buckling analysis of imperfect shells with stochastic non-Gaussian material and thickness properties," *International Journal of Solids and Structures*, vol. 46, no. 14-15, pp. 2800–2808, 2009.

[4] I. Elishakoff and J. Arbocz, "Reliability of axially compressed cylindrical shells with random axisymmetric imperfections," *International Journal of Solids and Structures*, vol. 18, no. 7, pp. 563–585, 1982.

[5] J. Arbocz and J. M. A. M. Hol, "Collapse of axially compressed cylindrical shells with random imperfections," *Thin-Walled Structures*, vol. 23, no. 1-4, pp. 131–158, 1995.

[6] V. Papadopoulos and P. Iglesis, "The effect of non-uniformity of axial loading on the buckling behaviour of shells with random imperfections," *International Journal of Solids and Structures*, vol. 44, no. 18-19, pp. 6299–6317, 2007.

[7] G. Ahmadi, "Stability of cylindrical shells subjected to random loadings," *Journal of Sound and Vibration*, vol. 107, no. 1, pp. 83–95, 1986.

[8] F. M. A. Silva, P. B. Gonçalves, and Z. J. G. N. del Prado, "Influence of physical and geometrical system parameters uncertainties on the nonlinear oscillations of cylindrical shells," *Journal of the Brazilian Society of Mechanical Sciences and Engineering*, vol. 34, no. 2, pp. 622–632, 2012.

[9] E. Capiez-Lernout, C. Soize, and M.-P. Mignolet, "Post-buckling nonlinear static and dynamical analyses of uncertain cylindrical shells and experimental validation," *Computer Methods in Applied Mechanics and Engineering*, vol. 271, pp. 210–230, 2014.

[10] D. Xiu and G. E. Karniadakis, "The Wiener-Askey polynomial chaos for stochastic differential equations," *SIAM Journal on Scientific Computing*, vol. 24, no. 2, pp. 619–644, 2002.

[11] K. Sepahvand, S. Marburg, and H.-J. Hardtke, "Uncertainty quantification in stochastic systems using polynomial chaos expansion," *International Journal of Applied Mechanics*, vol. 2, no. 2, pp. 305–353, 2010.

[12] O. G. Ernst, A. Mugler, H.-J. Starkloff, and E. Ullmann, "On the convergence of generalized polynomial chaos expansions," *ESAIM. Mathematical Modelling and Numerical Analysis*, vol. 46, no. 2, pp. 317–339, 2012.

[13] C. R. A. da Silva Jr. and A. T. Beck, "Bending of stochastic Kirchhoff plates on Winkler foundations via the Galerkin method and the Askey-Wiener scheme," *Probabilistic Engineering Mechanics*, vol. 25, no. 2, pp. 172–182, 2010.

[14] C. R. Á. da Silva Jr. and A. T. Beck, "Chaos-Galerkin solution of stochastic Timoshenko bending problems," *Computers & Structures*, vol. 89, no. 7-8, pp. 599–611, 2011.

[15] K. Sepahvand, S. Marburg, and H.-J. Hardtke, "Stochastic structural modal analysis involving uncertain parameters using generalized polynomial chaos expansion," *International Journal of Applied Mechanics*, vol. 3, no. 3, pp. 587–606, 2011.

[16] F. Santonja and B. Chen-Charpentier, "Uncertainty quantification in simulations of epidemics using polynomial chaos," *Computational and Mathematical Methods in Medicine*, vol. 2012, Article ID 742086, 8 pages, 2012.

[17] A. Desai and S. Sarkar, "Analysis of a nonlinear aeroelastic system with parametric uncertainties using polynomial chaos expansion," *Mathematical Problems in Engineering*, vol. 2010, Article ID 379472, 21 pages, 2010.

[18] J.-C. Cortés, J.-V. Romero, M.-D. Roselló, F.-J. Santonja, and R.-J. Villanueva, "Solving continuous models with dependent uncertainty: a computational approach," *Abstract and Applied Analysis*, vol. 2013, Article ID 983839, 10 pages, 2013.

[19] C. A. Schenk and G. I. Schuëller, "Buckling analysis of cylindrical shells with random geometric imperfections," *International Journal of Non-Linear Mechanics*, vol. 38, no. 7, pp. 1119–1132, 2003.

[20] V. Papadopoulos, D. C. Charmpis, and M. Papadrakakis, "A computationally efficient method for the buckling analysis of shells with stochastic imperfections," *Computational Mechanics*, vol. 43, no. 5, pp. 687–700, 2009.

[21] H. N. Chu, "Influence of large amplitudes on flexural vibrations of thin circular cylindrical shells," *Journal of Aerospace Science*, vol. 58, pp. 302–609, 1961.

[22] J. L. Nowinski, "Nonlinear transverse vibration of orthotropic cylindrical shells," *AIAA Journal*, vol. 1, no. 3, pp. 617–620, 1963.

[23] D. A. Evensen, "Some observations on the nonlinear vibration of thin cylindrical shells," *AIAA Journal*, vol. 1, no. 12, pp. 2857–2858, 1963.

[24] D. A. Evensen, "Nonlinear flexural vibrations of thin-walled circular cylinders," NASA TN, D-4090, National Aeronautics and Space Administration, 1967.

[25] M. D. Olson, "Some experimental observations on the nonlinear vibrations of cylindrical shells," *AIAA Journal*, vol. 3, no. 9, pp. 1775–1777, 1965.

[26] M. Amabili and M. P. Païdoussis, "Review of studies on geometrically nonlinear vibrations and dynamics of circular cylindrical shells and panels, with and without fluid-structure interaction," *Applied Mechanics Reviews*, vol. 56, no. 4, pp. 349–381, 2003.

[27] F. Alijani and M. Amabili, "Non-linear vibrations of shells: a literature review from 2003 to 2013," *International Journal of Non-Linear Mechanics*, vol. 58, pp. 233–257, 2014.

[28] D. O. Brush and B. O. Almroth, *Buckling of Bars, Plates and Shells*, McGraw-Hill, New York, NY, USA, 1st edition, 1975.

[29] N. Yamaki, *Elastic Stability of Circular Cylindrical Shell*, North-Holland, 27th edition, 1984.

[30] G. W. Hunt, K. A. J. Williams, and R. G. Cowell, "Hidden symmetry concepts in the elastic buckling of axially-loaded cylinders," *International Journal of Solids and Structures*, vol. 22, no. 12, pp. 1501–1515, 1986.

[31] P. B. Gonçalves and R. C. Batista, "Non-linear vibration analysis of fluid-filled cylindrical shells," *Journal of Sound and Vibration*, vol. 127, no. 1, pp. 133–143, 1988.

[32] P. B. Gonçalves and Z. J. G. N. Del Prado, "Nonlinear oscillations and stability of parametrically excited cylindrical shells," *Meccanica*, vol. 37, no. 6, pp. 569–597, 2002.

[33] P. B. Gonçalves, F. M. A. Silva, and Z. J. G. N. Del Prado, "Low-dimensional models for the nonlinear vibration analysis of cylindrical shells based on a perturbation procedure and proper orthogonal decomposition," *Journal of Sound and Vibration*, vol. 315, no. 3, pp. 641–663, 2008.

[34] F. M. A. Silva, P. B. Gonçalves, and Z. J. G. N. Del Prado, "An alternative procedure for the non-linear vibration analysis of fluid-filled cylindrical shells," *Nonlinear Dynamics*, vol. 66, no. 3, pp. 303–333, 2011.

[35] N. Wiener, "The homogeneous chaos," *American Journal of Mathematics*, vol. 60, no. 4, pp. 897–936, 1938.

[36] C. R. Á. da Silva Jr. and A. T. Beck, "Bending of stochastic Kirchhoff plates on Winkler foundations via the Galerkin method and the Askey-Wiener scheme," *Probabilistic Engineering Mechanics*, vol. 25, no. 2, pp. 172–182, 2010.

[37] C. R. A. Silva Jr., H. Azikri, G. E. Mantovani, and A. T. Beck, "Galerkin solution of stochastic beam bending on Winkler foundations," *Computer Modeling in Engineering and Sciences*, vol. 67, no. 2, pp. 119–149, 2010.

[38] P. B. Gonçalves and D. M. Santee, "Influence of uncertainties on the dynamic buckling loads of structures liable to asymmetric postbuckling behavior," *Mathematical Problems in Engineering*, vol. 2008, Article ID 490137, 24 pages, 2008.